

The Higgs Particle Mass, Width and Couplings

SCHUBERT, MICHAEL

Physikalisches Institut
Universität Freiburg

September 2, 2014



Abstract

This article presents an overview of the measurements of key features of the Higgs boson, including mass, width and coupling strengths. For the mass measurement the two important channels $H \rightarrow \gamma\gamma$ and $H \rightarrow Z \rightarrow 4\ell$ yield a mass of 125.36 ± 0.41 GeV. The width, while not directly measurable, can be constrained to be no more than 4 times the SM expectation. The coupling strengths for the various scenarios with SM or BSM contributions are all compatible with the SM expectations as well.

1 Introduction

The discovery of the Higgs boson at the LHC has answered many questions physicists had about the standard model but at the same time more questions cropped up. First and foremost the question: Is this really the standard model Higgs boson? Or maybe something else?

To answer these questions it is necessary to measure the properties of the particle. These properties are the mass, spin and CP state, the width and the couplings to other particles. Apart from the mass these are all fixed in the standard model, allowing comparison between theory and experiment. This article focuses on the mass, width and couplings. The spin and CP state are not discussed here, as the fixation of these to their standard model values is both justified and necessary for the determination of the coupling strengths.

As a reminder the Higgs production and decay processes are shown in fig.1 and fig.2

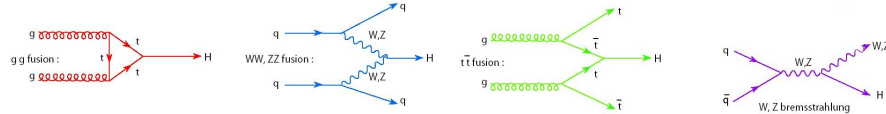


Figure 1: Feynman graphs of the important production modes of the Higgs boson: gluon-gluon fusion, vector boson fusion, $t\bar{t}$ fusion and associated production with a vector boson

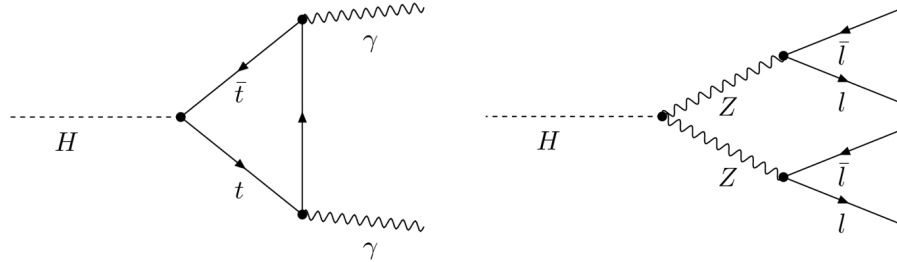


Figure 2: Example of the decay modes of the Higgs boson. The top in the loop can in principle be exchanged with any massive charged particle. The Z pair can be replaced by any massive particles with their respective decay products.

While the selection of the different decay channels is rather easy by looking for the signals of the corresponding decay products it is more complicated to separate the various production modes. As shown in fig.3 by the example of $H \rightarrow \gamma\gamma$ it is possible to enrich certain production modes by applying appropriate cuts. Knowing the cross section for these different selections the actual contributions of the different production modes can be inferred.

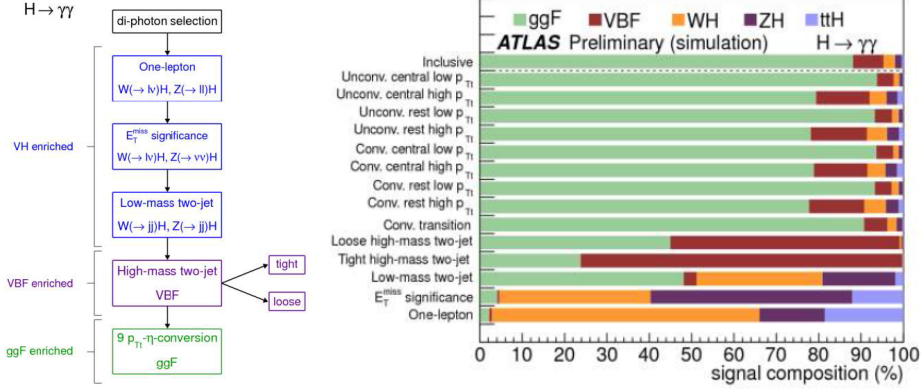


Figure 3: Example of the separation of production modes of the Higgs boson in the $\rightarrow \gamma\gamma$ channel. The variables used here will be explained later.

2 Mass

The mass is a very important feature of the Higgs boson, as it, once known, according to the standard model fixes every other property of the Higgs boson. It is therefore important to have a small error on this quantity. To this end the channels $H \rightarrow \gamma\gamma$ and $H \rightarrow Z \rightarrow 4\ell$ are used. Key feature of these channels are the clean final states consisting of only well understood objects: γ , e^\pm and μ^\pm . By use of well understood reference processes the detector response can be studied in great detail. The ATLAS collaboration uses more than 7 million events ($Z \rightarrow e^+e^-$, $Z \rightarrow \ell^+\ell^-\gamma$, $J/\psi \rightarrow e^+e^-$) to control the energy calibration, both global and cell specific, the behaviour of the different layers of the detector and the understanding of the material in front of the calorimeter for e^\pm and γ . Similarly the muon behaviour in the detector and muon spectrometer is monitored separately with about 15 million events (using $Z \rightarrow \mu^+\mu^-$, $J/\psi \rightarrow \mu^+\mu^-$). This results in a very low statistical uncertainty for measurements containing only these particles in the final state.

2.1 $H \rightarrow \gamma\gamma$

This channel is used because of the clean final state of two photons, allowing full reconstruction of the Higgs boson. Since photons, as mentioned, are well understood objects this results in a very good mass resolution. Another aspect is the smooth background that can be easily determined from the data. While this is not that important for the mass measurement itself, this was very important for the discovery of the Higgs boson. The ATLAS collaboration has split the analysis of this channel into 10 different categories. The categories are split for converted photons, different regions in the pseudo-

rapidity and different p_{Tt} ¹ regions. Since unconverted photons, meaning photons not having undergone pair production in the material in front of the calorimeter, provide a better energy resolution than converted ones, the different regions in the detector having different energy resolutions as well and the high p_{Tt} events yielding better energy resolution the splitting into the different categories improves the statistical error of the measurement. The different categories are shown in fig:4. The result can be seen in fig.5

Category	n_{sig}	FWHM [GeV]	σ_{eff} [GeV]	b in $\pm \sigma_{\text{eff}90}$	s/b [%]	s/\sqrt{b}
$\sqrt{s}=8 \text{ TeV}$						
Inclusive	402.	3.69	1.67	10670	3.39	3.50
Unconv. central low p_{Tt}	59.3	3.13	1.35	801	6.66	1.88
Unconv. central high p_{Tt}	7.1	2.81	1.21	26.0	24.6	1.26
Unconv. rest low p_{Tt}	96.2	3.49	1.53	2624	3.30	1.69
Unconv. rest high p_{Tt}	10.4	3.11	1.36	93.9	9.95	0.96
Unconv. transition	26.0	4.24	1.86	910	2.57	0.78
Conv. central low p_{Tt}	37.2	3.47	1.52	589	5.69	1.38
Conv. central high p_{Tt}	4.5	3.07	1.35	20.9	19.4	0.88
Conv. rest low p_{Tt}	107.2	4.23	1.88	3834	2.52	1.56
Conv. rest high p_{Tt}	11.9	3.71	1.64	144.2	7.44	0.89
Conv. transition	42.1	5.31	2.41	1977	1.92	0.85
$\sqrt{s}=7 \text{ TeV}$						
Inclusive	73.9	3.38	1.54	1752	3.80	1.59
Unconv. central low p_{Tt}	10.8	2.89	1.24	128	7.55	0.85
Unconv. central high p_{Tt}	1.2	2.59	1.11	3.7	30.0	0.58
Unconv. rest low p_{Tt}	16.5	3.09	1.35	363	4.08	0.78
Unconv. rest high p_{Tt}	1.8	2.78	1.21	13.6	11.6	0.43
Unconv. transition	4.5	3.65	1.61	125	3.21	0.36
Conv. central low p_{Tt}	7.1	3.28	1.44	105	6.06	0.62
Conv. central high p_{Tt}	0.8	2.87	1.25	3.5	21.6	0.40
Conv. rest low p_{Tt}	21.0	3.93	1.75	695	2.72	0.72
Conv. rest high p_{Tt}	2.2	3.43	1.51	24.7	7.98	0.40
Conv. transition	8.1	4.81	2.23	365	2.00	0.38

Figure 4: Tabel containing different features of signal and background for the different categories: expected number of signal events, expected FWHM of the signal, expected σ_{eff} =half the width containing 68% of the signal, expected background events in the region conaining 90% of the signal, and expected signal to background ratio.

Apart from the staticical uncertainties the systematic errors have to be accounted for as well. A summary of the systematic uncertainties is shown in fig.6. The excellent understanding of the detector can be seen there as the systematic uncertainty is never larger than 0.6%. This then amounts to a measured mass of $m_H = 125.98 \pm 0.42(\text{stat}) \pm 0.28(\text{syst})\text{GeV}$. A signal strength² can be extracted as well and is measured to be $\mu = 1.29 \pm 0.30$.

¹ $p_{Tt} = \left| \left(p_T^{\gamma_1} + p_T^{\gamma_2} \right) \times \frac{p_T^{\gamma_1} - p_T^{\gamma_2}}{|p_T^{\gamma_1} - p_T^{\gamma_2}|} \right|$, this is the projection of transverse momentum transvere to the transverse thrust axis, the transverse thrust axis being the axis maximizing the transverse momentum projected onto it

²The signal strength is the cross section normalized to the SM expectation.

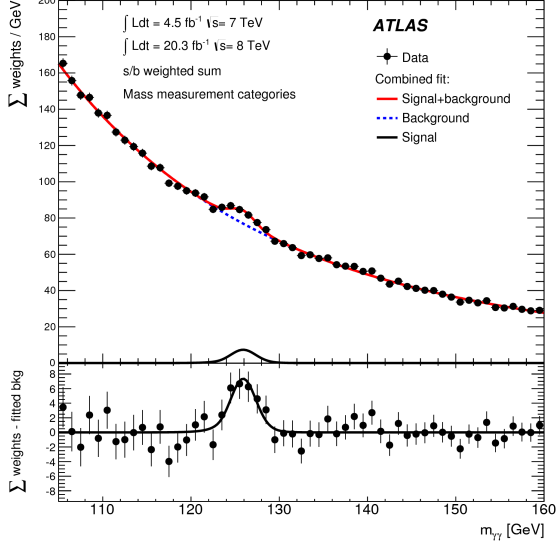


Figure 5: Result for the $H \rightarrow \gamma\gamma$ channel, for illustration purposes each category is weighted by its signal to background ratio.

Class	Unconverted				Converted					
	Central		Rest		Trans.	Central		Rest		Trans.
	low p_{Ti}	high p_{Ti}	low p_{Ti}	high p_{Ti}		low p_{Ti}	high p_{Ti}	low p_{Ti}	high p_{Ti}	
$Z \rightarrow e^+e^-$ calibration	0.02	0.03	0.04	0.04	0.11	0.02	0.02	0.05	0.05	0.11
LAr cell non-linearity	0.12	0.19	0.09	0.16	0.39	0.09	0.19	0.06	0.14	0.29
Layer calibration	0.13	0.16	0.11	0.13	0.13	0.07	0.10	0.05	0.07	0.07
ID material	0.06	0.06	0.08	0.08	0.10	0.05	0.05	0.06	0.06	0.06
Other material	0.07	0.08	0.14	0.15	0.35	0.04	0.04	0.07	0.08	0.20
Conversion reconstruction	0.02	0.02	0.03	0.03	0.05	0.03	0.02	0.05	0.04	0.06
Lateral shower shape	0.04	0.04	0.07	0.07	0.06	0.09	0.09	0.18	0.19	0.16
Background modeling	0.10	0.06	0.05	0.11	0.16	0.13	0.06	0.14	0.18	0.20
Vertex measurement						0.03				
Total	0.23	0.28	0.24	0.30	0.59	0.21	0.25	0.27	0.33	0.47

Figure 6: Tabel of the relative systematic uncertainties in % for the different categories.

2.2 $H \rightarrow ZZ^* \rightarrow 4\ell$

As before this channel provides a clean final state. The two Z bosons decaying into e^\pm and/or μ^\pm allow the full reconstruction of the Higgs boson. The leptons in the final state being well understood then results in a good mass resolution. In addition to that this channel features a good signal to background ratio.

The analysis of this channel is split into 4 different categories by the ATLAS collaboration, simply separating the different lepton decay possibilities of the Z bosons. Fig.7 shows the different categories and the respective expected and observed number of events.

This then results in the invariant 4 lepton mass distribution shown in fig.8. Also shown there is the result of a boosted decision tree for better distinguishability of signal and

Final state	Signal full mass range	Signal	ZZ^*	$Z + \text{jets}, t\bar{t}$	s/b	Expected	Observed
$\sqrt{s} = 7 \text{ TeV}$ 4.5 fb^{-1}							
4μ	1.00 ± 0.10	0.91 ± 0.09	0.46 ± 0.02	0.10 ± 0.04	1.7	1.47 ± 0.10	2
$2e2\mu$	0.66 ± 0.06	0.58 ± 0.06	0.32 ± 0.02	0.09 ± 0.03	1.5	0.99 ± 0.07	2
$2\mu2e$	0.50 ± 0.05	0.44 ± 0.04	0.21 ± 0.01	0.36 ± 0.08	0.8	1.01 ± 0.09	1
$4e$	0.46 ± 0.05	0.39 ± 0.04	0.19 ± 0.01	0.40 ± 0.09	0.7	0.98 ± 0.10	1
Total	2.62 ± 0.26	2.32 ± 0.23	1.17 ± 0.06	0.96 ± 0.18	1.1	4.45 ± 0.30	6
$\sqrt{s} = 8 \text{ TeV}$ 20.3 fb^{-1}							
4μ	5.80 ± 0.57	5.28 ± 0.52	2.36 ± 0.12	0.69 ± 0.13	1.7	8.33 ± 0.6	12
$2e2\mu$	3.92 ± 0.39	3.45 ± 0.34	1.67 ± 0.08	0.60 ± 0.10	1.5	5.72 ± 0.37	7
$2\mu2e$	3.06 ± 0.31	2.71 ± 0.28	1.17 ± 0.07	0.36 ± 0.08	1.8	4.23 ± 0.30	5
$4e$	2.79 ± 0.29	2.38 ± 0.25	1.03 ± 0.07	0.35 ± 0.07	1.7	3.77 ± 0.27	7
Total	15.6 ± 1.6	13.8 ± 1.4	6.24 ± 0.34	2.00 ± 0.28	1.7	22.1 ± 1.5	31
$\sqrt{s} = 7 \text{ TeV}$ and $\sqrt{s} = 8 \text{ TeV}$							
4μ	6.80 ± 0.67	6.20 ± 0.61	2.82 ± 0.14	0.79 ± 0.13	1.7	9.81 ± 0.64	14
$2e2\mu$	4.58 ± 0.45	4.04 ± 0.40	1.99 ± 0.10	0.69 ± 0.11	1.5	6.72 ± 0.42	9
$2\mu2e$	3.56 ± 0.36	3.15 ± 0.32	1.38 ± 0.08	0.72 ± 0.12	1.5	5.24 ± 0.35	6
$4e$	3.25 ± 0.34	2.77 ± 0.29	1.22 ± 0.08	0.76 ± 0.11	1.4	4.75 ± 0.32	8
Total	18.2 ± 1.8	16.2 ± 1.6	7.41 ± 0.40	2.95 ± 0.33	1.6	26.5 ± 1.7	37

Figure 7: Expected and observed number of events for the different categories.

background. This BDT uses p_T , η and D_{ZZ}^3 as input variables. This can be condensed into a log-likelihood plot as seen in fig.9. As a result in this channel a mass of $m_H = 124.51 \pm 0.52(\text{stat}) \pm 0.06(\text{syst})\text{GeV}$ and a signal strength of $\mu = 1.66^{+0.45}_{-0.38}$ is measured.

2.3 Combination

The two channels presented, $H \rightarrow \gamma\gamma$ and $H \rightarrow ZZ^* \rightarrow 4\ell$, each yielded a mass for the Higgs boson. With a measured mass difference of $\Delta m_H = 1.47 \pm 0.67(\text{stat}) \pm 0.28(\text{syst})\text{GeV}$ these measurements agree to 2σ and can be combined to the final result of $m_H = 125.36 \pm 0.37(\text{stat}) \pm 0.18(\text{syst})\text{GeV}$. Fig.10 shows this combination. Since both measurements have been performed with the same detector the systematic uncertainties are correlated. Fig.11 shows these uncertainties, showing once again the good understanding the ATLAS collaboration has of their detector.

³ $D_{ZZ} = \log \frac{|\mathcal{M}_{\text{sig}}|^2}{|\mathcal{M}_{ZZ}|^2}$, the \mathcal{M} are the matrix elements of signal and ZZ background respectively

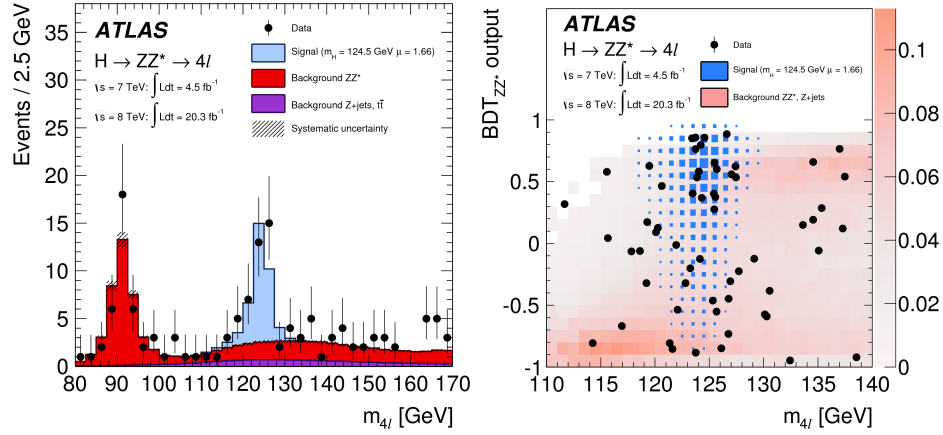


Figure 8: Result of the $H \rightarrow ZZ^* \rightarrow 4\ell$ channel. Left: Invariant 4 lepton mass distribution, Right: Mass distribution against the BDT output.

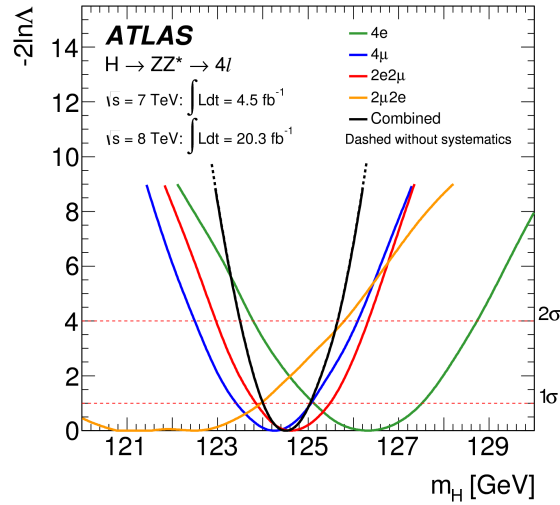


Figure 9: Log-likelihood ratio for the different categories and the combination.

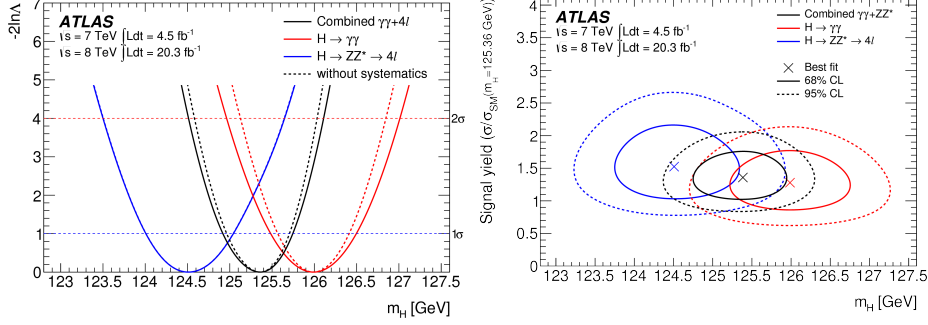


Figure 10: Left: Likelihood ratio for both channels and their combination. Right: Higgs boson mass plotted against the signal yield for both channels and the combination with uncertainty contours.

Systematic	Uncertainty on m_H [MeV]
LAr syst on material before presampler (barrel)	70
LAr syst on material after presampler (barrel)	20
LAr cell non-linearity (layer 2)	60
LAr cell non-linearity (layer 1)	30
LAr layer calibration (barrel)	50
Lateral shower shape (conv)	50
Lateral shower shape (unconv)	40
Presampler energy scale (barrel)	20
ID material model ($ \eta < 1.1$)	50
$H \rightarrow \gamma\gamma$ background model (unconv rest low p_{Tr})	40
$Z \rightarrow ee$ calibration	50
Primary vertex effect on mass scale	20
Muon momentum scale	10
Remaining systematic uncertainties	70
Total	180

Figure 11: Break down of the systematic uncertainties involved in the mass measurement of the Higgs boson

3 Width

The measurement of the decay width of the Higgs boson is difficult. The experimental energy resolution on an event to event basis is about 2GeV, the uncertainty of the mass measurement as already seen is about 0.4GeV. This is still more than 2 orders of magnitude greater than the theory prediction of about 4MeV, leaving no hope to directly measure the width of the Higgs boson. It is however possible to infer an upper bound on the width of the Higgs boson. By assuming the Higgs boson to behave exactly as predicted in the standard model, with no other contributions from any BSM theory, the exact shape of the Higgs boson cross section as a function of center of mass energy is known once the mass is known. By comparing the on and off resonance cross sections the total width can be inferred. The CMS collaboration did just that, measuring the width to be smaller than 4 times its SM expectation value. However,

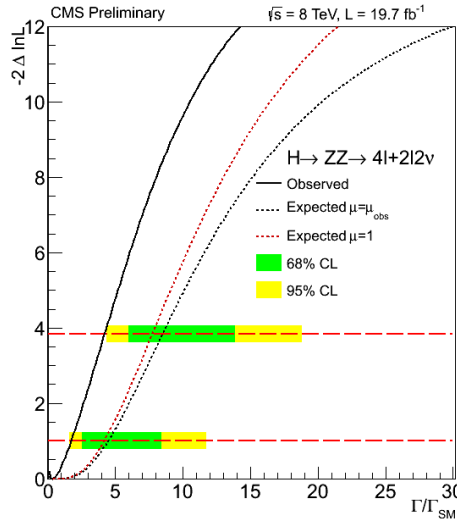


Figure 12: Upper limit on the Higgs boson decay width over the SM expectation, as measured by the CMS collaboration.

since the width measurement included the assumption of a SM Higgs boson, there is no model independent way to measure the total width of the Higgs boson. The variables left are signal strengths and relative coupling strengths.

4 Couplings

To start the measurement of the coupling behaviour of the Higgs boson a few basic assumptions are needed. These assumptions greatly simplify the computation of the desired quantities. First it is assumed that everything observed originated from the same particle, excluding several particles of similar mass that just can't be resolved. Second is the assumption of the examined particle to have a vanishing decay width.

This is a reasonable assumption as explained in the previous section and greatly simplifies the dependencies of desired variables on measured quantities. And last is the assumption of the particle being a CP-even scalar, since the event topology is used in the distinction of the production processes. This is reasonable as well seeing as other measurements not presented here support that theory.

With these assumptions in place the modified coupling strength is introduced. Every vertex factor of a vertex coupling to the Higgs boson is simply multiplied by the coupling strength κ_X for the coupling to particle X as shown in fig.13. By construction this factor is 1 for the SM expectation. Furthermore care has to be taken whether this vertex is the production or decay vertex of the Higgs boson. Since only certain production processes are possible, a simple κ_X is enough. For the decay however coupling any possible particle has to be considered, requiring the normalization to the total width of the Higgs boson, signified by κ_H . Although the SM predicts the functional dependence of κ_H off the κ_X for the different particles, this is the only way to model independently describe the modified coupling. In the example shown in fig.14 this is illustrated. However in that case the loop coupling to the photons can not only contain t but also W^\pm leading to interference effects. For this an effective coupling of the Higgs boson to photons is introduced, with theory giving the functional dependence:

$$\kappa_\gamma^2(\kappa_F \kappa_V) = 1.59\kappa_V^2 - 0.66\kappa_V \kappa_F + 0.07\kappa_F^2$$

Since the coupling strength modifies the matrix element which only holds physical meaning when squared, the sign of the coupling strength is irrelevant. The relative sign of two coupling strengths however is important in interference effects, making this the only possibility to infer the relative sign of the coupling strength of bosons and fermions. Since only the relative sign is important, κ_V is set to be positive.

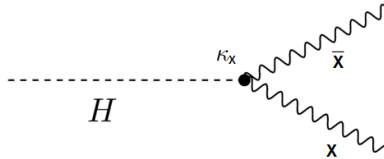


Figure 13: Feynman graph of a Higgs boson vertex with indicated modified coupling.

4.1 Coupling strength

Here the assumption is made that any modification to the coupling is uniform for bosons and fermions respectively, meaning only one coupling strength describing the interaction of the Higgs boson with vector bosons and one for the interaction with fermions and the effective coupling to gluons:

$$\begin{aligned} \kappa_V &= \kappa_W = \kappa_Z \\ \kappa_F &= \kappa_t = \kappa_b = \kappa_\tau = \kappa_g \end{aligned}$$

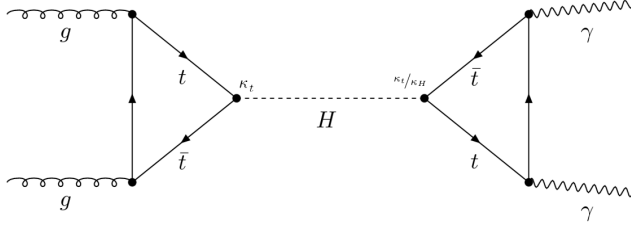


Figure 14: Feynman graph of the $gg \rightarrow H \rightarrow \gamma\gamma$ via two t loops. Considering this process alone the matrix element is to be modified by κ_t^2/κ_H

4.1.1 SM contributions only

Here it is assumed that, apart from the modified coupling strength, the Higgs boson behaves exactly as predicted by the SM, coupling only to SM particles. Then the total width of the Higgs boson can be expressed by the other coupling strengths

$$\kappa_H = 0.75\kappa_F^2 + 0.25\kappa_V^2$$

This then results in the following functional dependence of the cross section and branching ratio:

$$\begin{aligned} \sigma(gg \rightarrow H) \times BR(H \rightarrow \gamma\gamma) &\sim \frac{\kappa_F^2 \kappa_\gamma^2(\kappa_F, \kappa_V)}{0.75\kappa_F^2 + 0.25\kappa_V^2} \\ \sigma(qq' \rightarrow qq'H) \times BR(H \rightarrow \gamma\gamma) &\sim \frac{\kappa_V^2 \kappa_\gamma^2(\kappa_F, \kappa_V)}{0.75\kappa_F^2 + 0.25\kappa_V^2} \\ \sigma(gg \rightarrow H) \times BR(H \rightarrow ZZ^{(*)}, H \rightarrow WW^{(*)}) &\sim \frac{\kappa_F^2 \kappa_V^2}{0.75\kappa_F^2 + 0.25\kappa_V^2} \\ \sigma(qq' \rightarrow qq'H) \times BR(H \rightarrow ZZ^{(*)}, H \rightarrow WW^{(*)}) &\sim \frac{\kappa_V^2 \kappa_V^2}{0.75\kappa_F^2 + 0.25\kappa_V^2} \\ \sigma(qq' \rightarrow qq'H, VH) \times BR(H \rightarrow \tau\tau, H \rightarrow b\bar{b}) &\sim \frac{\kappa_V^2 \kappa_F^2}{0.75\kappa_F^2 + 0.25\kappa_V^2} \end{aligned}$$

Utilizing this the ATLAS collaboration produced values of $\kappa_F = 1.15 \pm 0.08$ and $\kappa_V = 0.99_{-0.15}^{+0.17}$ for the coupling strengths. As can be seen in fig.15, the relative sign of the coupling strengths is preferred to be positive, as per SM expectation, but a negative relative sign is not yet excluded.

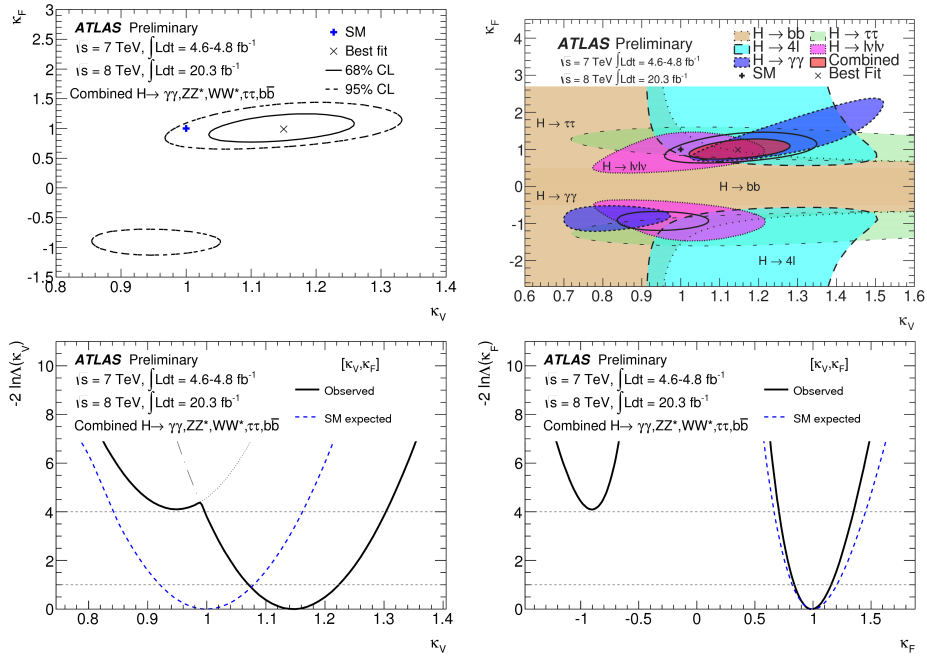


Figure 15: Contour and log likelihood plots for the coupling strengths with SM assumptions.

4.1.2 Free total width

In this scenario the total width of the Higgs boson is not assumed to behave to SM expectation making it an additional free parameter. This means that only the ratio of coupling strengths is now measurable. With the new variables $\kappa_{VV} = \kappa_V \kappa_V / \kappa_H$ and $\lambda_{FV} = \kappa_F / \kappa_V$ the functional dependence of cross section and branching ratio is changed to

$$\begin{aligned}\sigma(gg \rightarrow H) \times BR(H \rightarrow \gamma\gamma) &\sim \lambda_{FV}^2 \kappa_{VV}^2 \kappa_\gamma^2(\lambda_{FV}, 1) \\ \sigma(qq' \rightarrow qq'H) \times BR(H \rightarrow \gamma\gamma) &\sim \kappa_{VV}^2 \kappa_\gamma^2(\lambda_{FV}, 1) \\ \sigma(gg \rightarrow H) \times BR(H \rightarrow ZZ^{(*)}, H \rightarrow WW^{(*)}) &\sim \lambda_{FV}^2 \kappa_{VV}^2 \\ \sigma(qq' \rightarrow qq'H) \times BR(H \rightarrow ZZ^{(*)}, H \rightarrow WW^{(*)}) &\sim \kappa_{VV}^2 \\ \sigma(qq' \rightarrow qq'H, VH) \times BR(H \rightarrow \tau\tau, H \rightarrow b\bar{b}) &\sim \kappa_{VV}^2 \lambda_{FV}^2\end{aligned}$$

With this the ATLAS collaboration measured $\lambda_{FV} = 0.86^{+0.14}_{-0.12}$ and $\kappa_{VV} = 1.28^{+0.16}_{-0.15}$. Once again the negative relative sign of the coupling strengths is disfavoured but not excluded, as can be seen in fig.16.

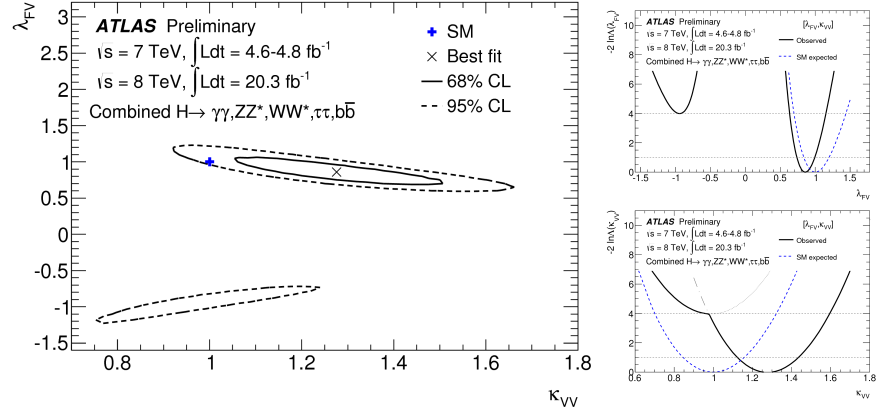


Figure 16: Contour and log likelihood plots for the coupling strength ratios with total width as free parameter.

4.1.3 Free loop contents

In addition to the free total width the loop content is now no longer set to SM expectations. This makes the effective coupling to the photon an additional free parameter and since this was used to determine the relative sign earlier, that is no longer possible. The new variables are

$$\begin{aligned}\lambda_{FV} &= \kappa_F/\kappa_V \\ \lambda_{\gamma V} &= \kappa_\gamma/\kappa_V \\ \kappa_{VV} &= \kappa_V \kappa_V / \kappa_H\end{aligned}$$

Leading to the following dependencies

$$\begin{aligned}\sigma(gg \rightarrow H) \times BR(H \rightarrow \gamma\gamma) &\sim \lambda_{FV}^2 \kappa_{VV}^2 \lambda_{\gamma V}^2 \\ \sigma(qq' \rightarrow qq' H) \times BR(H \rightarrow \gamma\gamma) &\sim \kappa_{VV}^2 \lambda_{\gamma V}^2 \\ \sigma(gg \rightarrow H) \times BR(H \rightarrow ZZ^{(*)}, H \rightarrow WW^{(*)}) &\sim \lambda_{FV}^2 \kappa_{VV}^2 \\ \sigma(qq' \rightarrow qq' H) \times BR(H \rightarrow ZZ^{(*)}, H \rightarrow WW^{(*)}) &\sim \kappa_{VV}^2 \\ \sigma(qq' \rightarrow qq' H, VH) \times BR(H \rightarrow \tau\tau, H \rightarrow b\bar{b}) &\sim \kappa_{VV}^2 \lambda_{FV}^2\end{aligned}$$

The result of this measurement by the ATLAS cooperation is $\lambda_{FV} = 0.85^{+0.23}_{-0.13}$, $\lambda_{\gamma V} = 1.22^{+0.18}_{-0.14}$ and $\kappa_{VV} = 1.15 \pm 0.21$. As mentioned and seen in fig.17 the relative sign information is lost.

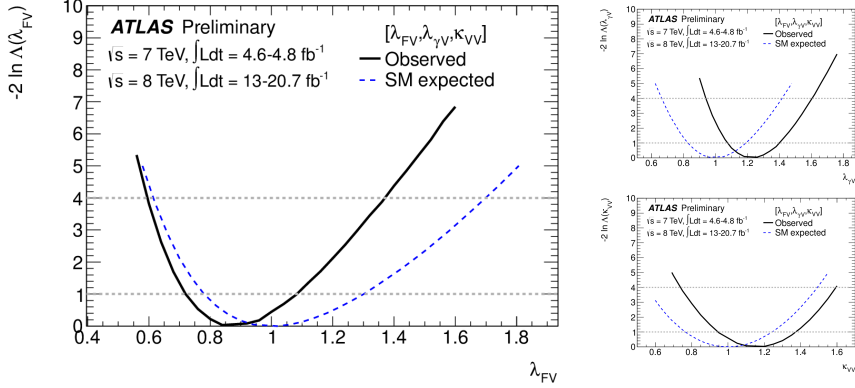


Figure 17: Log likelihood plots for the coupling strength ratios with total width and loop content as free parameters.

4.2 Custodial symmetry

Custodial symmetry refers to the requirement of the coupling strength modifier of the W and Z boson to be equal. This is required by theory and can be tested by introducing an additional free parameter. Instead of having one parameter for the coupling to vector bosons there are now two parameters, one for each the coupling to the W and the Z boson. In addition the vector boson fusion process is now dependent on these two coupling strengths. As with the effective coupling to the photon the functional dependence is predicted by theory, leaving a $\kappa_{VBF}^2(\kappa_W, \kappa_Z)$.

4.2.1 Free total width

In this case similar to before no assumptions about the total width of the Higgs bosons are made, introducing this as a free parameter. As earlier this means that only ratios of coupling strengths can be measured. With these variables

$$\begin{aligned}\kappa_{ZZ} &= \kappa_Z \kappa_Z / \kappa_H \\ \lambda_{WZ} &= \kappa_W / \kappa_Z \\ \lambda_{FZ} &= \kappa_F / \kappa_Z\end{aligned}$$

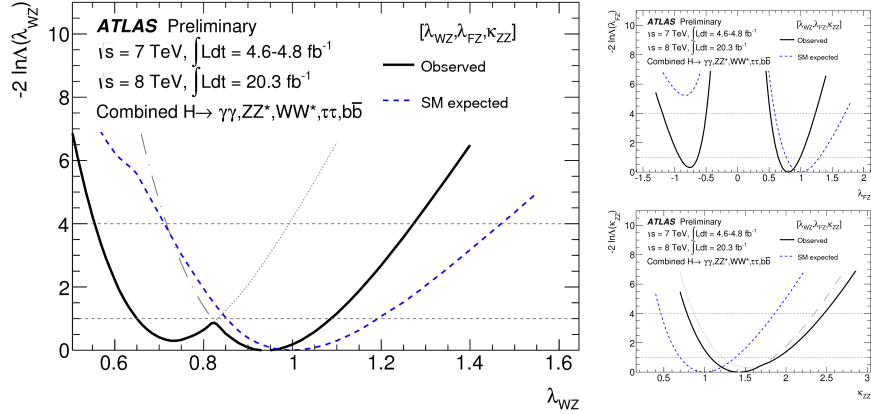


Figure 18: Log likelihood plots for the coupling strength ratios with total width as free parameter, probing custodial symmetry.

the dependencies look like this

$$\begin{aligned}
\sigma(gg \rightarrow H) \times BR(H \rightarrow \gamma\gamma) &\sim \lambda_{FZ}^2 \kappa_{ZZ}^2 \kappa_\gamma^2(\lambda_{FZ}, 1) \\
\sigma(qq' \rightarrow qq'H) \times BR(H \rightarrow \gamma\gamma) &\sim \kappa_{VBF}^2(\lambda_{WZ}, 1) \kappa_{ZZ}^2 \kappa_\gamma^2(\lambda_{FZ}, 1) \\
\sigma(gg \rightarrow H) \times BR(H \rightarrow ZZ^{(*)}) &\sim \lambda_{FZ}^2 \kappa_{ZZ}^2 \\
\sigma(qq' \rightarrow qq'H) \times BR(H \rightarrow ZZ^{(*)}) &\sim \kappa_{VBF}^2(\lambda_{WZ}, 1) \kappa_{ZZ}^2 \\
\sigma(gg \rightarrow H) \times BR(H \rightarrow WW^{(*)}) &\sim \lambda_{FZ}^2 \kappa_{ZZ}^2 \lambda_{WZ}^2 \\
\sigma(qq' \rightarrow qq'H) \times BR(H \rightarrow WW^{(*)}) &\sim \kappa_{VBF}^2(\lambda_{WZ}, 1) \kappa_{ZZ}^2 \lambda_{WZ}^2 \\
\sigma(qq' \rightarrow qq'H, VH) \times BR(H \rightarrow \tau\tau, H \rightarrow b\bar{b}) &\sim \kappa_{VBF}^2(\lambda_{WZ}, 1) \kappa_{ZZ}^2 \lambda_{FZ}^2
\end{aligned}$$

The results are $\lambda_{WZ} = 0.94^{+0.14}_{-0.29}$, $\lambda_{FZ} \in [-0.91, -0.63] \cup [0.65, 1.00]$ and $\kappa_{ZZ} = 1.41^{+0.49}_{-0.34}$. In this case, as seen in fig.18, there is no preferred relative sign of vector boson (Z in this case) and fermion coupling.

4.2.2 Free loop content

Once again it is of interest to not constrain the content of the loop and introduce a separate effective coupling of the Higgs boson to photons. By doing this the relative sign information of vector boson and fermion coupling is lost. The variables are

$$\begin{aligned}
\kappa_{ZZ} &= \kappa_Z \kappa_Z / \kappa_H \\
\lambda_{WZ} &= \kappa_W / \kappa_Z \\
\lambda_{\gamma Z} &= \kappa_\gamma / \kappa_Z \\
\lambda_{FZ} &= \kappa_F / \kappa_Z
\end{aligned}$$

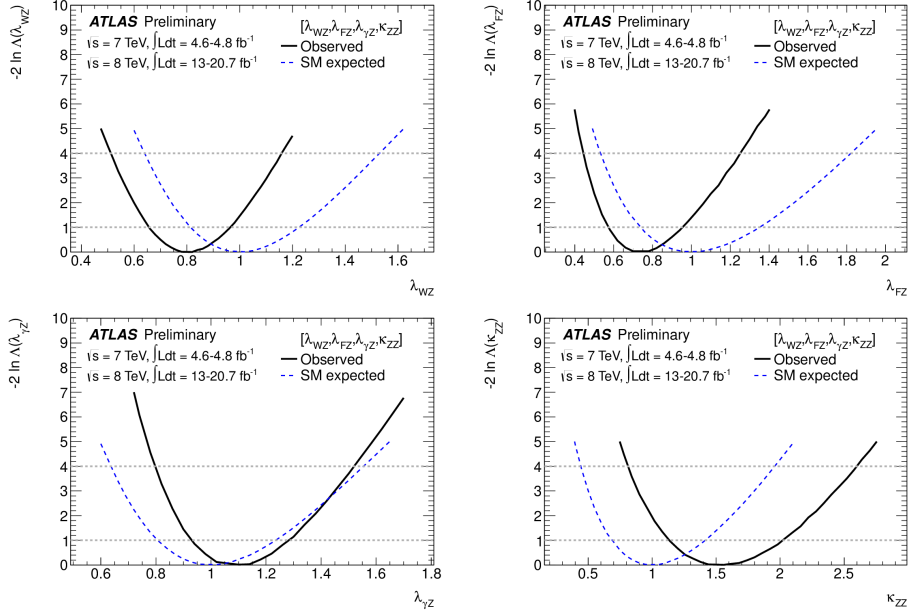


Figure 19: Log likelihood plots for the coupling strength ratios with total width and loop content as free parameters, probing custodial symmetry.

leading to these functionalities

$$\begin{aligned}
&\sigma(gg \rightarrow H) \times BR(H \rightarrow \gamma\gamma) \sim \lambda_{FZ}^2 \kappa_{ZZ}^2 \lambda_{\gamma Z}^2 \\
&\sigma(qq' \rightarrow qq'H) \times BR(H \rightarrow \gamma\gamma) \sim \kappa_{VBF}^2(\lambda_{WZ}, 1) \kappa_{ZZ}^2 \lambda_{\gamma Z}^2 \\
&\sigma(gg \rightarrow H) \times BR(H \rightarrow ZZ^{(*)}) \sim \lambda_{FZ}^2 \kappa_{ZZ}^2 \\
&\sigma(qq' \rightarrow qq'H) \times BR(H \rightarrow ZZ^{(*)}) \sim \kappa_{VBF}^2(\lambda_{WZ}, 1) \kappa_{ZZ}^2 \\
&\sigma(gg \rightarrow H) \times BR(H \rightarrow WW^{(*)}) \sim \lambda_{FZ}^2 \kappa_{ZZ}^2 \lambda_{WZ}^2 \\
&\sigma(qq' \rightarrow qq'H) \times BR(H \rightarrow WW^{(*)}) \sim \kappa_{VBF}^2(\lambda_{WZ}, 1) \kappa_{ZZ}^2 \lambda_{WZ}^2 \\
&\sigma(qq' \rightarrow qq'H, VH) \times BR(H \rightarrow \tau\tau, H \rightarrow b\bar{b}) \sim \kappa_{VBF}^2(\lambda_{WZ}, 1) \kappa_{ZZ}^2 \lambda_{FZ}^2
\end{aligned}$$

The results are $\lambda_{WZ} = 0.80 \pm 0.15$, $\lambda_{FZ} = 0.74^{+0.21}_{-0.17}$, $\lambda_{\gamma Z} = 1.10 \pm 0.18$ and $\kappa_{ZZ} = 1.5^{+0.5}_{-0.4}$ with the log likelihood plots shown in fig.19

4.3 Loop contents

Another point of interest is the question of what actually appears in the loops coupling the Higgs boson to the massless gluons and photons. Since these cannot be measured directly an effective coupling of the Higgs boson to these bosons is introduced.

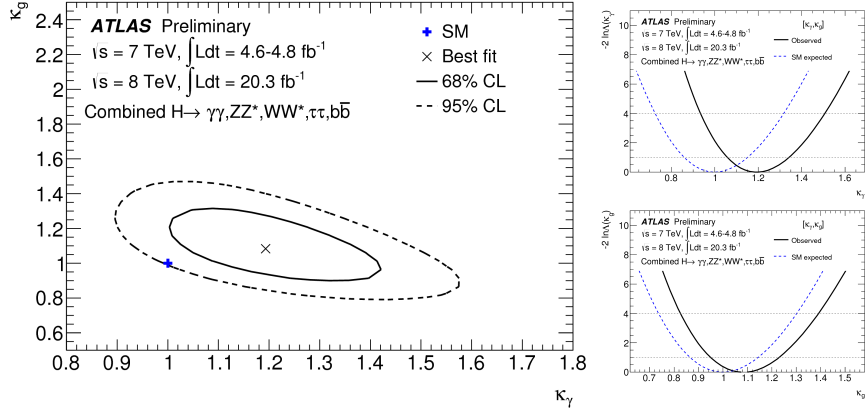


Figure 20: *Contour and log likelihood plots for the effective coupling strengths to gluons and photons.*

4.3.1 SM loop contents

Here the behaviour of the Higgs boson is set to the SM expectations with the exception of the effective coupling to gluons and photons. This means the Higgs boson only couples to SM particles with the predicted strengths. This especially means that the functional dependencies of the total width of the Higgs boson are known:

$$\kappa_H = 0.085\kappa_g^2 + 0.0023\kappa_\gamma^2 + 0.91$$

With this the dependencies of cross section and branching ratio are as follows:

$$\begin{aligned} \sigma(gg \rightarrow H) \times BR(H \rightarrow \gamma\gamma) &\sim \frac{\kappa_g^2 \kappa_\gamma^2}{0.085\kappa_g^2 + 0.0023\kappa_\gamma^2 + 0.91} \\ \sigma(qq' \rightarrow qq'H) \times BR(H \rightarrow \gamma\gamma) &\sim \frac{\kappa_\gamma^2}{0.085\kappa_g^2 + 0.0023\kappa_\gamma^2 + 0.91} \\ \sigma(gg \rightarrow H) \times BR(H \rightarrow ZZ^{(*)}, H \rightarrow WW^{(*)}) &\sim \frac{\kappa_g^2}{0.085\kappa_g^2 + 0.0023\kappa_\gamma^2 + 0.91} \\ \sigma(qq' \rightarrow qq'H) \times BR(H \rightarrow ZZ^{(*)}, H \rightarrow WW^{(*)}) &\sim \frac{1}{0.085\kappa_g^2 + 0.0023\kappa_\gamma^2 + 0.91} \\ \sigma(qq' \rightarrow qq'H, VH) \times BR(H \rightarrow \tau\tau, H \rightarrow b\bar{b}) &\sim \frac{1}{0.085\kappa_g^2 + 0.0023\kappa_\gamma^2 + 0.91} \end{aligned}$$

The results here are $\kappa_g = 1.08^{+0.15}_{-0.13}$ and $\kappa_\gamma = 1.19^{+0.15}_{-0.12}$. The plots are shown in fig.20.

4.3.2 BSM contributions

Now it is assumed that there are explicit BSM contributions resulting in either invisible or undetectable decays of the Higgs boson. To account for that the expression for total

width is modified:

$$\Gamma_H = \frac{\kappa_H^2(\kappa_i)}{1 - BR_{\text{inv,undet}}} \Gamma_H^{\text{SM}}$$

Leading to

$$\begin{aligned} \sigma(gg \rightarrow H) \times BR(H \rightarrow \gamma\gamma) &\sim \frac{\kappa_g^2 \kappa_\gamma^2}{0.085\kappa_g^2 + 0.0023\kappa_\gamma^2 + 0.91} (1 - BR_{\text{inv,undet}}) \\ \sigma(qq' \rightarrow qq'H) \times BR(H \rightarrow \gamma\gamma) &\sim \frac{\kappa_\gamma^2}{0.085\kappa_g^2 + 0.0023\kappa_\gamma^2 + 0.91} (1 - BR_{\text{inv,undet}}) \\ \sigma(gg \rightarrow H) \times BR(H \rightarrow ZZ^{(*)}, H \rightarrow WW^{(*)}) &\sim \frac{\kappa_g^2}{0.085\kappa_g^2 + 0.0023\kappa_\gamma^2 + 0.91} (1 - BR_{\text{inv,undet}}) \\ \sigma(qq' \rightarrow qq'H) \times BR(H \rightarrow ZZ^{(*)}, H \rightarrow WW^{(*)}) &\sim \frac{1}{0.085\kappa_g^2 + 0.0023\kappa_\gamma^2 + 0.91} (1 - BR_{\text{inv,undet}}) \\ \sigma(qq' \rightarrow qq'H, VH) \times BR(H \rightarrow \tau\tau, H \rightarrow b\bar{b}) &\sim \frac{1}{0.085\kappa_g^2 + 0.0023\kappa_\gamma^2 + 0.91} (1 - BR_{\text{inv,undet}}) \end{aligned}$$

and resulting in $\kappa_g = 1.00^{+0.23}_{-0.16}$, $\kappa_\gamma = 0.94^{+0.16}_{-0.13}$ and $BR_{\text{inv,undet}} = -0.16^{+0.29}_{-0.30}$. In fig.21 the plot for the branching ratio for invisible/undetectable events turns up twice, where one has $BR_{\text{inv,undet}}$ constrained to be positive to give an accurate upper bound for it.

5 Conclusion

The mass of the Higgs boson has been measured to be $m_H = 125.36 \pm 0.41 \text{ GeV}$ by the ATLAS collaboration with a signal strength of $\mu = 1.30 \pm 0.20$. The couplings of the Higgs boson have been examined as well, resulting in a summary plot shown in fig.22. With these figures the standard model has been validated within 2 standard deviations. The CMS collaboration has produced similar results with a mass of $m_H = 125.03^{+0.26}_{-0.27} (\text{stat})^{+0.13}_{-0.15} (\text{syst})$ and couplings measurements (see fig.23) agreeing with the SM expectations.

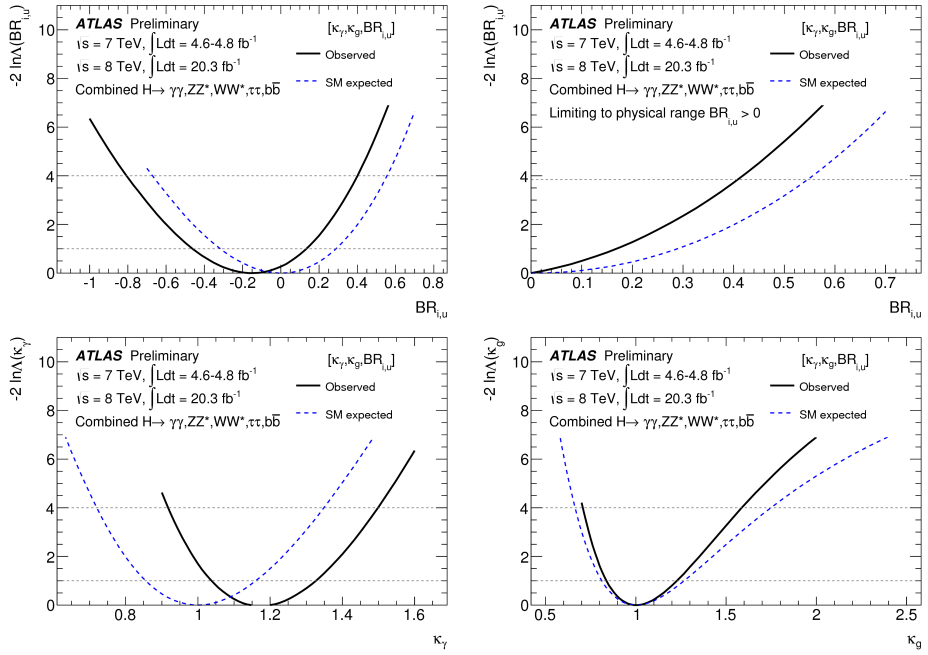


Figure 21: Log likelihood plots for the effective coupling strengths and the branching ratio for invisible/undetectable events.

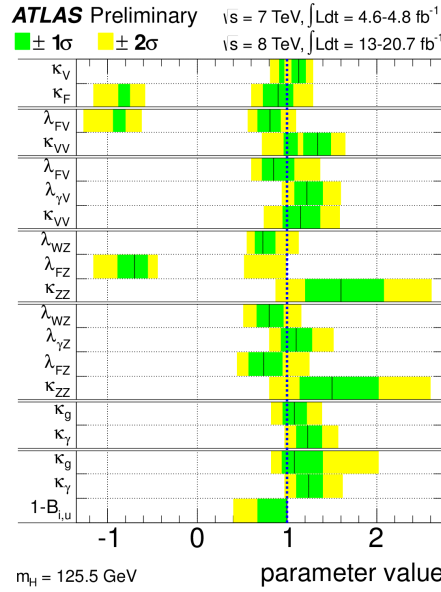


Figure 22: Summary of the couplings measurements done by the ATLAS collaboration.

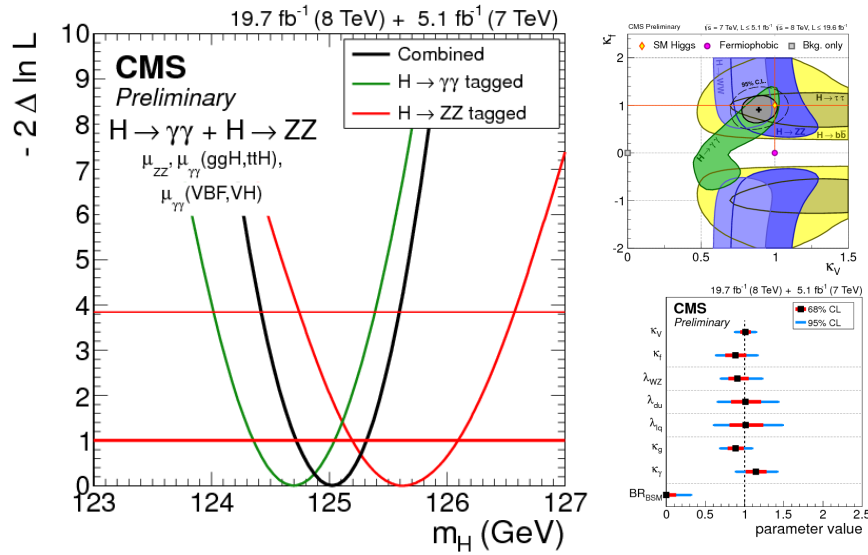


Figure 23: Results of the CMS collaboration. Left: Log likelihood plot for the mass measurement. Top right: Contour plot of vector boson and fermion coupling strength. Bottom right: Summary plot for the couplings measurements.

6 References

References

- [1] ATLAS Collaboration, *Measurement of the Higgs boson mass from the $H \rightarrow \gamma\gamma$ and $H \rightarrow ZZ^{(*)}4\ell$ channels with the ATLAS detector using 25 fb^{-1} of pp collision data*, arXiv:1406.3827v1, 15. Jun 2014
- [2] ATLAS Collaboration, *Combined coupling measurement of the Higgs-like boson with the ATLAS detector using up to 25 fb^{-1} of proton-proton collision data*, ATLAS-CONF-2013-034, 13. Mar 2013
- [3] ATLAS Collaboration, *Updated coupling measurement of the Higgs-like boson with the ATLAS detector using up to 25 fb^{-1} of proton-proton collision data*, ATLAS-CONF-2014-009, 20. Mar 2014
- [4] ATLAS Collaboration, *Measurement of Higgs boson production and couplings in diboson final states with the ATLAS detector at the LHC*, Physics Letters B 726 (2013) 88-119, Aug 2013
- [5] CMS Collaboration, *Measurement of the properties of the new boson with a mass near 125 GeV*, CMS PAS HIG-13-005, 17. Apr 2013
- [6] CMS Collaboration, *Constraints on the Higgs boson width from off-shell production and decay of Z-boson pairs*, arXiv:1405.3455v1, 14. May 2014